Supplementary Materials for

Computational modeling of aberrant electrical activity following remuscularization with intramyocardially injected pluripotent stem cell-derived cardiomyocytes

Joseph K. Yu[1,2,5*], Jialiu A. Liang[1], Seth H. Weinberg[3,4], Natalia A. Trayanova[1,2,5]

[1]Department of Biomedical Engineering, Johns Hopkins University
3400 N Charles Street, 208 Hackerman, Baltimore, MD
[2]Department of Medicine, Johns Hopkins University School of Medicine, Baltimore, MD
[3]Department of Biomedical Engineering, The Ohio State University, Columbus, OH
[4]Davis Heart and Lung Research Institute
The Ohio State University Wexner Medical Center, Columbus, OH
[5]Alliance for Cardiovascular Diagnostic and Treatment Innovation (ADVANCE)
Johns Hopkins University, 3400 N Charles Street, 216 Hackerman, Baltimore, MD

*To whom correspondence should be addressed; E-mail: jyu78@jhmi.edu

Detailed Methods

Computational model

The model for electrical conduction along a linear strand of myocytes integrating gap junctional (GJ) and ephaptic coupling was modified from those of several previous publications [1–3]. Each myocyte was idealized as a symmetric cylinder and discretized into 6 patches: 4 axial and 2 disc (junctional) patches, one at each end of the cell (Fig. 1A). Adult ventricular myocytes (length: 100 μm, radius: 11 μm) were larger than graft PSC-CMs (length: 100 μm,

radius: between 6-11 μm) with sodium channels (NaChs) distributed nonuniformly. specifically, 90% of NaChs were localized at the disc patches. To achieve this, 45% of maximum g_{Na} conductance (total g_{Na} was fixed across the entire cell) was allocated to each of the two disc patches; the remaining 10% was distributed across the 4 remaining axial patches. In PSC-CMs, NaChs were either distributed uniformly or nonuniformly, the former simulating a more immature cytoarchitecture.

Each myocyte patch generated capacitive and ionic currents proportional to the membrane surface area of the patch. In host ventricular myocytes, the ionic currents were represented by the Luo-Rudy phase I (LR1) ventricular myocyte model equations [4]. The net ionic flux across each membrane patch $j \in \{1, \ldots, 6\}$ in myocyte i was described by 6 distinct ionic currents

$$I_{ion}^{(i,j)} = I_{Na}^{(i,j)} + I_{si}^{(i,j)} + I_{K}^{(i,j)} + I_{K1}^{(i,j)} + I_{Kp}^{(i,j)} + I_{b}^{(i,j)} \tag{1}$$

From left to right, the ionic currents on the right hand side are the sodium current, slow inward (calcium) current, potassium current, inward-rectifier potassium current, plateau potassium current, and background Ohmic current. In graft PSC-CMs, a constant depolarizing current (I_d) was introduced to the LR1 model as previously described[5, 6]. Thus, the net ionic flux was described as

$$I_{ion}^{(i,j)} = I_{Na}^{(i,j)} + I_{si}^{(i,j)} + I_{K}^{(i,j)} + I_{K1}^{(i,j)} + I_{Kp}^{(i,j)} + I_{b}^{(i,j)} + I_{d}^{(i,j)} \tag{2}$$

The value of I_d determined the rate of spontaneous beating (Figure S1). Parameters for host and graft myocytes are given in Table 1.

Transmembrane potentials ($V_m^{(i,j)}$) were computed at nodes corresponding to each membrane patch (Fig. 1B, 1C) utilizing the methodology described by Tsumoto *et. al.* [3, 7] but with slight modifications. Complete mathematical derivations can be found in . Briefly, myoplasmic resistances between adjacent axial nodes and between adjacent axial and disc nodes

were $R_{myo} = p_{myo}L_p/(\pi r^2)$ and $\frac{1}{2}R_{myo}$, respectively. To represent GJ coupling, nodes corresponding to disc patches of abutting myocytes were connected by a gap junctional resistance, R_{gap}. A simple two-state dynamic gating model [8] was implemented to represent voltage-dependent gating of GJs such that R_{gap} changed with time. Intercellular voltage differences had the effect of increasing R_{gap}. The gating variable between myocytes i and $i+1$ were governed by the following set of equations

$$\frac{dg^{i,i+1}}{dt} = \frac{g_\infty(V_j^{i,i+1}) - g^{i,i+1}}{\tau_g(V_j^{i,i+1})} \tag{3}$$

$$g_\infty(V_j^{i,i+1}) = g_{min} + \frac{g_{max} - g_{min}}{1 + \exp\left(A_g(|V_j^{i,i+1}| - V_g)\right)} \tag{4}$$

$$\tau_g(V_j^{i,i+1}) = \frac{1}{\sigma_g \exp\left(k_g|V_j^{i,i+1}|\right)}. \tag{5}$$

The variables g_∞ and τ_g are functions of intercellular voltage difference between myocytes i and $i+1$ ($V_j^{i,i+1} = V_m^{(i,6)} - V_m^{(i+1,1)}$). Model parameters can be found in Table 2. To represent ephaptic coupling, the potential of the junctional space at the intercalated disc (ID) between abutting myocytes was represented by an additional node. This junctional node was connected to all nodes of abutting myocytes sharing the same junctional space (axial resistances each $\frac{1}{2}R_{cl}$) and bulk extracellular space (radial resistance, R_{radial}) with a T-shaped network of resistances (Fig. 1B, 1C). We assumed that the junctional spaces had a cylindrical shape; the radius of a particular junctional space would be equal to that of the largest myocyte at the specific ID. The axial ($\frac{1}{2}R_{cl}$) and radial (R_{radial}) resistances depended on the width (w) and radius (r) of the junctional space ($R_{cl} = \rho_{ext}w/(\pi r^2)$; $R_{radial} = \rho_{ext}/(8\pi w)$ [9]). A value of 150 Ohms $\cdot$ cm was used for the extracellular resistivity, ρ_{ext}.

Of the ionic species, the LR1 model only accounts for dynamic changes in intracellular Ca^{2+} ($[Ca_i^{2+}]$) concentration. Within a membrane patch j of an individual myocyte j, the dynamics

of $[Ca_i^{2+}]$ was governed by

$$\frac{d[Ca_i^{2+}]^{(i,j)}}{dt} = \frac{-A^{(i,j)} I_{si}^{(i,j)}}{2FV^{(i,j)}} + \frac{[Ca_i^{2+}]^{(i,j-1)} - [Ca_i^{2+}]^{(i,j)}}{\tau_{Ca}} + \frac{[Ca_i^{2+}]^{(i,j+1)} - [Ca_i^{2+}]^{(i,j)}}{\tau_{Ca}} \quad (6)$$

$A^{(i,j)}$ and $V^{(i,j)}$ are the surface area and volume, respectively, of a given membrane patch. For disc patches, $A^{(i,j)} = \pi r^2$ and $V^{(i,j)} = L_p \pi r^2/2$; for axial patches, $A^{(i,j)} = 2\pi r L_p$ and $V^{(i,j)} = L_p \pi r^2$. The time constant τ_{Ca} determines the rate of ionic transfer between membrane patches and is computed as $\tau_{Ca} = L_p^2/(2D_{Ca})$ where $D_{Ca} = 0.25$ ms [2]. No intercellular ionic flux was assumed.

Numerical integration

Numerical integration was carried out similar to several previous publications [1, 2] with slight modifications. The transmembrane potential across all membrane patches was integrated at a higher temporal resolution than the gating variables and ionic concentrations. First, the ionic currents and change in gating variable values were computed for each membrane patch at each discrete point in time t. Over the time interval $\Delta t_1 = 5$ µs, we assumed that changes in the membrane currents and gating variables were negligible and thus constant. By applying Kirchoff's Voltage Law (KVL) and Kirchoff's Current Law (KCL) (see for detailed derivations), a set of coupled first-order differential equations with constant coefficients that described the change in transmembrane potential across all membrane patches was obtained; an implicit integration method was used to solve this system with a time step of $\Delta t_2 = \Delta t_1/10 = 0.5$ µs. Specifically, the linear relationship was

$$\left(\mathbf{I} - \Delta t_2 \mathbf{C_m^{-1} R^{-1} L}\right) \mathbf{V_m}^{k+1} = \mathbf{V_m}^{k} + \Delta t_2 \mathbf{C_m^{-1} I_{ion}} \quad (7)$$

where $\mathbf{I}$ is a $np \times np$ identity matrix, $\mathbf{C_m}$ is a $np \times np$ diagonal matrix where each diagonal entry corresponds to the membrane capacitance of a particular myocyte patch, $\mathbf{R}$ is the resistance

matrix, $\mathbf{L}$ is the Laplacian matrix that denotes how individual myocyte nodes are resistively coupled to one another (see for additional details). Once transmembrane potentials were updated for $t + \Delta t_1$, ionic concentrations and gating variables across all membrane patches and gating variables across all GJs were numerically integrated using a forward Euler method. Explicitly, the membrane kinetic gating variables $g_m \in \{m, h, j, d, f, x\}$ were computed as

$$\mathbf{g_m}^{k+1} = \mathbf{g_m}^{k} + \Delta t_1 \dot{\mathbf{g}}_{\mathbf{m}}^{k}(\mathbf{g_m}^{k}, \mathbf{V_m}^{k}) \tag{8}$$

where $\mathbf{g_{m,k}}$ is the $np \times 6$ matrix of the membrane gating variables, and $\dot{\mathbf{g}}_{\mathbf{m}}^{k}(\mathbf{g_m}^{k}, \mathbf{V_m}^{k})$ is the corresponding vector of derivatives. Similarly, the GJ gating variables were computed as,

$$\mathbf{g}^{k+1} = \mathbf{g}^{k} + \Delta t_1 \dot{\mathbf{g}}^{k}(\mathbf{g}^{k}, \mathbf{V_j}^{k}) \tag{9}$$

$[Ca_i^{2+}]$ across all myocyte patches was computed as

$$[\mathbf{Ca_i^{2+}}]^{k+1} = [\mathbf{Ca_i^{2+}}]^{k} + \Delta t_1 \Big(\frac{-1}{z_{Ca} F} \mathbf{V_{vol}^{-1}} \mathbf{I_{si}} + \frac{1}{\tau_{Ca}} \mathbf{L_{Ca}} [\mathbf{Ca_i^{2+}}]^{k} \Big) \tag{10}$$

where $z_{Ca} = 2$, F is Faraday's constant, $\mathbf{V_{vol}}$ is a $np \times np$ diagonal matrix where each diagonal entry corresponds to a particular membrane patch volume, $\mathbf{I_{si}}$ is a $np \times 1$ vector of I_{si} across all membrane patches, and $\mathbf{L_{Ca}}$ is the Laplacian matrix taking into account no intercellular flux.

$$\mathbf{L_{Ca}} = \left[\begin{array}{c|c|c|c} \begin{matrix} -1 & 1 & 0 & 0 & 0 & 0 \\ 1 & -2 & 1 & 0 & 0 & 0 \\ 0 & 1 & -2 & 1 & 0 & 0 \\ 0 & 0 & 1 & -2 & 1 & 0 \\ 0 & 0 & 0 & 1 & -2 & 1 \\ 0 & 0 & 0 & 0 & 1 & -1 \end{matrix} & \mathbf{0} & \mathbf{0} & \mathbf{0} \\ \hline \mathbf{0} & \ddots & \mathbf{0} & \mathbf{0} \\ \hline \mathbf{0} & \mathbf{0} & \begin{matrix} -1 & 1 & 0 & 0 & 0 & 0 \\ 1 & -2 & 1 & 0 & 0 & 0 \\ 0 & 1 & -2 & 1 & 0 & 0 \\ 0 & 0 & 1 & -2 & 1 & 0 \\ 0 & 0 & 0 & 1 & -2 & 1 \\ 0 & 0 & 0 & 0 & 1 & -1 \end{matrix} & \mathbf{0} & \mathbf{0} \\ \hline \mathbf{0} & \mathbf{0} & \mathbf{0} & \ddots & \mathbf{0} \\ \hline \mathbf{0} & \mathbf{0} & \mathbf{0} & \mathbf{0} & \begin{matrix} -1 & 1 & 0 & 0 & 0 & 0 \\ 1 & -2 & 1 & 0 & 0 & 0 \\ 0 & 1 & -2 & 1 & 0 & 0 \\ 0 & 0 & 1 & -2 & 1 & 0 \\ 0 & 0 & 0 & 1 & -2 & 1 \\ 0 & 0 & 0 & 0 & 1 & -1 \end{matrix} \end{array}\right] \tag{11}$$

Quantification of synchrony

The population beating synchrony across all graft PSC-CMs was quantified by the Z statistic[10]. Z was computed as the time average of instantaneous z statistics (z_t) or

$$Z = \sum_{t=t_0}^{T} z_t \tag{12}$$

Each z_t was defined as the beating synchrony across a given population of N PSC-CMs at time t. Specifically,

$$z_t = \frac{1}{N}\left|\sum_{j=1}^{N} e^{i\theta_j}\right| \tag{13}$$

where θ_j is the phase of a particular myocyte j. For each myocyte j, the phase at time t was computed as $\theta_j = 2\pi x_j$, where x_j is defined as the progression through the current cycle length at time t (i.e., bounded on the interval $[0, 1]$); cycle lengths were defined as the interval between adjacent upstrokes of spontaneous beats. The values of z_t are bounded on the interval $[0, 1]$; a value of $z_t = 1$ indicates complete synchrony (i.e., myocyte phases θ_j are all equal) while a value of $z_t = 0$ indicates complete asynchrony (i.e., uniform distribution of myocyte phases).

Quantification of conduction velocity

Conduction velocity (CV) across the myocardial strand was computed by linear regression of the activation times of myocytes $\frac{N}{4}$ and $\frac{3N}{4}$ as previously described[2], where N is the number of myocytes in the linear strand. Activation times were defined as when transmembrane potential crosses above $-60mV$.

Mathematical derivations

We shall present a derivation of the generalized form of the resistance matrix **R** used to simulate electrical impulse propagation across a one-dimensional myofiber strand. The derivation differs slightly from those detailed in Tsumoto *et. al.*[3, 7] due to how the potential drop between gap junctionally-coupled myocytes was computed. From the equivalent circuits in Fig. 1B,1C, one can derive a system of equations using Ohm's Law, Kirchoff's Voltage Law (KVL), and Kirchoff's Current Law (KCL). This results in the following linear relationship,

$$\mathbf{RI} = \mathbf{V}, \tag{14}$$

where **R** is a $pn \times pn$ square matrix, **I** and **V** are $pn \times 1$ column vectors, and p and n are the number of patches per myocyte and the number of myocytes in the myofiber, respectively. Each vector entry in **I** and **V** corresponds to a particular intracellular patch node $j \in \{1, \ldots, p\}$ in

myocyte $i \in \{1, \ldots, n\}$, or

$$\mathbf{V} = \left[\begin{array}{cccc|c|cccc} v^{(1,1)} & v^{(1,2)} & \cdots & v^{(1,p)} & \cdots & \cdots & v^{(n,1)} & v^{(n,2)} & \cdots & v^{(n,p)} \end{array} \right]^{\mathsf{T}} \tag{15}$$

$$\mathbf{I} = \left[\begin{array}{cccc|c|cccc} i^{(1,1)} & i^{(1,2)} & \cdots & i^{(1,p)} & \cdots & \cdots & i^{(n,1)} & i^{(n,2)} & \cdots & i^{(n,p)} \end{array} \right]^{\mathsf{T}} \tag{16}$$

For the current vector $\mathbf{I}$, each entry corresponded to the current flowing from each intracellular node to its membrane segment; for the voltage vector $\mathbf{V}$, each entry corresponded to the net potential drop across the specific node.

To derive the full matrix form, we consider three distinct types of myocyte membrane patches:

1. Axial patches only adjacent to other axial patches: $j \in \{3, \ldots, p-2\}$,
2. Axial patches adjacent to a disc patch and an axial patch: $j \in \{2, p-1\}$, and
3. Disc patches: $j \in \{1, p\}$.

For the first case, we apply KCL and Ohm's Law and obtain:

$$i^{(i,j)} = i^{(i,j-1)} + i^{(i,j+1)} \tag{17}$$

$$= \frac{\phi_i^{(i,j-1)} - \phi_i^{(i,j)}}{R_{myo}} + \frac{\phi_i^{(i,j+1)} - \phi_i^{(i,j)}}{R_{myo}} \tag{18}$$

$$-i^{(i,j)} R_{myo} = -\phi_i^{(i,j-1)} + 2\phi_i^{(i,j)} - \phi_i^{(i,j+1)} \tag{19}$$

For the second case, we apply KCL and Ohm's law again for two subcases: the disc patch adjacent to the axial patch being considered is (a) not coupled or (b) is coupled to a disc patch of another myocyte. For (a), we obtain

$$i^{(i,2)} = i^{(i,1)} + i^{(i,3)} \tag{20}$$

$$= \frac{\phi_i^{(i,1)} - \phi_i^{(i,2)}}{\frac{1}{2} R_{myo}} + \frac{\phi_i^{(i,3)} - \phi_i^{(i,2)}}{R_{myo}} \tag{21}$$

$$-i^{(i,2)} R_{myo} = -2\phi_i^{(i,1)} + 3\phi_i^{(i,2)} - \phi_i^{(i,3)} \tag{22}$$

$$-i^{(i,2)} R_{myo} = -2V_m^{(i,1)} + 3V_m^{(i,2)} - V_m^{(i,3)}. \tag{23}$$

The last line is obtained from the fact that $V_m = \phi_i - \phi_e$ and $\phi_e = 0$ in the bulk interstitial space. By myocyte symmetry,

$$-i^{(i,p-1)}R_{myo} = -2V_m^{(i,p)} + 3V_m^{(i,p-1)} - V_m^{(i,p-2)}. \tag{24}$$

For (b), we obtain,

$$-i^{(i,2)}R_{myo} = -2\phi_i^{(i,1)} + 3\phi_i^{(i,2)} - \phi_i^{(i,3)} \tag{25}$$

$$= -2(\phi_e^{(i,1)} - V_m^{(i,1)}) + 3V_m^{(i,2)} - V_m^{(i,3)} \tag{26}$$

Using KCL and Ohm's law applied at the cleft, we obtain an expression for $\phi_e^{(i,1)}$ to be:

$$\phi_e^{(i,1)} = i^{(i-1,p)}R_{radial} + i^{(i,1)}(R_{radial} + \tfrac{1}{2}R_{cl}) \tag{27}$$

Substituting equation 27 into equation 26 and rearranging, we obtain

$$i^{(i-1,p)}(2R_{radial}) + i^{(i,1)}(2R_{radial} + R_{cl}) - i^{(i,2)}R_{myo} = -2V_m^{(i,1)} + 3V_m^{(i,2)} - V_m^{(i,3)} \tag{28}$$

By myocyte symmetry,

$$i^{(i+1,1)}(2R_{radial}) + i^{(i,p)}(2R_{radial} + R_{cl}) - i^{(i,p-1)}R_{myo} = -2V_m^{(i,p)} + 3V_m^{(i,p-1)} - V_m^{(i,p-2)} \tag{29}$$

For the third and final case, we again consider two subcases: the disc patch being considered is (a) not coupled or (b) is coupled to a another disc patch of another myocyte. For the first, we obtain

$$i^{(i,1)} = \frac{\phi_i^{(i,2)} - \phi_i^{(i,1)}}{\frac{1}{2}R_{myo}} \tag{30}$$

$$-i^{(i,1)}\tfrac{1}{2}R_{myo} = \phi_i^{(i,1)} - \phi_i^{(i,2)} \tag{31}$$

For (b), we first apply KVL at the cleft between myocytes i and $i-1$ and collect terms to obtain

$$0 = i^{(i-1,p)}R_{radial} + i^{(i,1)}(R_{radial} + \tfrac{1}{2}R_{cl} + \tfrac{1}{2}R_{myo}) - i_{i-1,i}^{gap}(\tfrac{1}{2}R_{myo}) + V_m^{(i,1)} - V_m^{(i,2)}. \tag{32}$$

The term $i_{i-1,i}^{gap}$ is the GJ current between the myocytes and is

$$i_{i-1,i}^{gap} = \frac{\phi_i^{(i-1,p)} - \phi_i^{(i,1)}}{R_{gap}^{i-1,i}} = \frac{V_m^{(i-1,p)} - V_m^{(i,1)} + \phi_e^{(i-1,p)} - \phi_e^{(i,1)}}{R_{gap}^{i-1,i}} \tag{33}$$

where $R_{gap}^{i-1,i}$ is the GJ resistance between myocytes i and $i-1$. Using KVL, we obtain equations for $\phi_e^{(i-1,p)}$ and $\phi_e^{(i,1)}$ as

$$\phi_e^{(i,1)} = i^{(i-1,p)} R_{radial} + i^{(i,1)}(R_{radial} + \tfrac{1}{2}R_{cl}) \tag{34}$$

$$\phi_e^{(i-1,p)} = i^{(i,1)} R_{radial} + i^{(i-1,p)}(R_{radial} + \tfrac{1}{2}R_{cl}) \tag{35}$$

Combining equations 33 - 35 into equation 32 and rearranging, we obtain

$$\begin{aligned} - i^{(i-1,p)}\left(R_{radial} - \tfrac{R_{myo}R_{cl}}{4R_{gap}^{i-1,i}}\right) - i^{(i,1)}\left(R_{radial} + \tfrac{1}{2}R_{cl} + \tfrac{1}{2}R_{myo} + \tfrac{R_{myo}R_{cl}}{4R_{gap}^{i-1,i}}\right) \\ = -V_m^{(i-1,p)}\left(\tfrac{R_{myo}}{2R_{gap}^{i-1,i}}\right) + V_m^{(i,1)}\left(1 + \tfrac{R_{myo}}{2R_{gap}^{i-1,i}}\right) - V_m^{(i,1)} \end{aligned} \tag{36}$$

And by symmetry again,

$$\begin{aligned} - i^{(i,1)}\left(R_{radial} - \tfrac{R_{myo}R_{cl}}{4R_{gap}^{i-1,i}}\right) - i^{(i-1,p)}\left(R_{radial} + \tfrac{1}{2}R_{cl} + \tfrac{1}{2}R_{myo} + \tfrac{R_{myo}R_{cl}}{4R_{gap}^{i-1,i}}\right) \\ = -V_m^{(i,1)}\left(\tfrac{R_{myo}}{2R_{gap}^{i-1,i}}\right) + V_m^{(i-1,p)}\left(1 + \tfrac{R_{myo}}{2R_{gap}^{i-1,i}}\right) - V_m^{(i-1,p)} \end{aligned} \tag{37}$$

The sets of equations 19, 23, 28, 29, 31, 36, 37 form the linear system $\mathbf{RI} = \mathbf{V}$. For a linear homogeneous myofiber where the number of myocyte patches $p = 6$, the resistance matrix $\mathbf{R}$ is

described by

$$
\left[\begin{array}{cccccc|ccc|cc|cccccc}
R_5 & 0 & 0 & 0 & 0 & 0 & & & & & & & & & & \\
0 & R_0 & 0 & 0 & 0 & 0 & & & & & & & & & & \\
0 & 0 & R_0 & 0 & 0 & 0 & & & & & & & & & & \\
0 & 0 & 0 & R_0 & 0 & 0 & & & \mathbf{0} & & \mathbf{0} & & & & \mathbf{0} & \\
0 & 0 & 0 & 0 & R_0 & R_2 & R_4 & & & & & & & & & \\
0 & 0 & 0 & 0 & 0 & R_1 & R_3 & & & & & & & & & \\
\hline
 & & & & & R_3 & R_1 & & & & & & & & & \\
 & & & & & \vdots & & \ddots & & & \mathbf{0} & & & & \mathbf{0} & \\
 & & & & & & & & R_1 & R_3 & & & & & & \\
\hline
 & & & & & & R_3 & R_1 & 0 & 0 & 0 & 0 & 0 & 0 & & \\
 & & & & & & R_4 & R_2 & R_0 & 0 & 0 & 0 & 0 & 0 & & \\
 & & & \mathbf{0} & & & & 0 & 0 & R_0 & 0 & 0 & 0 & 0 & \mathbf{0} & \\
 & & & & & & & 0 & 0 & 0 & R_0 & 0 & 0 & 0 & & \\
 & & & & & & & 0 & 0 & 0 & 0 & R_0 & R_2 & R_4 & & \\
 & & & & & & & 0 & 0 & 0 & 0 & 0 & R_1 & R_3 & & \\
\hline
 & & & & & & & & & & & & R_3 & R_1 & & \\
 & & & \mathbf{0} & & & \mathbf{0} & & & & & & \vdots & \ddots & & \\
 & & & & & & & & & & & & & & R_1 & R_3 \\
\hline
 & & & & & & & & & & & & & R_3 & R_1 & 0 & 0 & 0 & 0 & 0 \\
 & & & & & & & & & & & & & R_4 & R_2 & R_0 & 0 & 0 & 0 & 0 \\
 & & & \mathbf{0} & & & \mathbf{0} & & & \mathbf{0} & & & & & 0 & 0 & R_0 & 0 & 0 & 0 \\
 & & & & & & & & & & & & & & 0 & 0 & 0 & R_0 & 0 & 0 \\
 & & & & & & & & & & & & & & 0 & 0 & 0 & 0 & R_0 & 0 \\
 & & & & & & & & & & & & & & 0 & 0 & 0 & 0 & 0 & R_5
\end{array}\right] \tag{38}
$$

where

$$R_0 = -R_{myo} \tag{39}$$

$$R_1 = -\left(R_{radial} + \tfrac{1}{2}R_{cl} + \tfrac{1}{2}R_{myo} + \tfrac{R_{myo}R_{cl}}{4R_{gap}}\right) \tag{40}$$

$$R_2 = 2R_{radial} + R_{cl} \tag{41}$$

$$R_3 = -\left(R_{radial} - \tfrac{R_{myo}R_{cl}}{4R_{gap}}\right) \tag{42}$$

$$R_4 = 2R_{radial} \tag{43}$$

$$R_5 = -R_{myo}/2 \tag{44}$$

The voltage vector $\mathbf{V}$ can be computed using the following relationship

$$\mathbf{V} = \mathbf{L}\mathbf{V}_\mathbf{m} \tag{45}$$

where $\mathbf{L}$ is a $pn \times pn$ Laplacian matrix. In this particular case, $\mathbf{L}$ is defined as

$$\left[\begin{array}{c|c|c|c|c}
\begin{array}{cccccc} 1 & -1 & 0 & 0 & 0 & 0 \\ -2 & 3 & -1 & 0 & 0 & 0 \\ 0 & -1 & 2 & -1 & 0 & 0 \\ 0 & 0 & -1 & 2 & -1 & 0 \\ 0 & 0 & 0 & -2 & 3 & -1 \\ 0 & 0 & 0 & 0 & -1 & \alpha \end{array} & \begin{array}{c} \\ \\ \\ \\ \\ \beta \end{array} & \mathbf{0} & \mathbf{0} & \mathbf{0} \\ \hline
\begin{array}{r} \beta \\ \\ \\ \end{array} & \begin{array}{ccc} \alpha & & \\ & \ddots & \\ & & \alpha \end{array} & \begin{array}{l} \\ \\ \beta \end{array} & \mathbf{0} & \mathbf{0} \\ \hline
\mathbf{0} & \begin{array}{r} \beta \\ \\ \\ \\ \\ \\ \end{array} & \begin{array}{cccccc} \alpha & -1 & 0 & 0 & 0 & 0 \\ -2 & 3 & -1 & 0 & 0 & 0 \\ 0 & -1 & 2 & -1 & 0 & 0 \\ 0 & 0 & -1 & 2 & -1 & 0 \\ 0 & 0 & 0 & -2 & 3 & -1 \\ 0 & 0 & 0 & 0 & -1 & \alpha \end{array} & \begin{array}{l} \\ \\ \\ \\ \\ \beta \end{array} & \mathbf{0} \\ \hline
\mathbf{0} & \mathbf{0} & \begin{array}{r} \beta \\ \\ \\ \end{array} & \begin{array}{ccc} \alpha & & \\ & \ddots & \\ & & \alpha \end{array} & \begin{array}{l} \\ \\ \beta \end{array} \\ \hline
\mathbf{0} & \mathbf{0} & \mathbf{0} & \begin{array}{r} \beta \\ \\ \\ \\ \\ \\ \end{array} & \begin{array}{cccccc} \alpha & -1 & 0 & 0 & 0 & 0 \\ -2 & 3 & -1 & 0 & 0 & 0 \\ 0 & -1 & 2 & -1 & 0 & 0 \\ 0 & 0 & -1 & 2 & -1 & 0 \\ 0 & 0 & 0 & -2 & 3 & -1 \\ 0 & 0 & 0 & 0 & -1 & 1 \end{array}
\end{array}\right] \tag{46}$$

where $\alpha = 1 + \frac{R_{myo}}{2R_{gap}}$, $\beta = -\frac{R_{myo}}{2R_{gap}}$, and $\mathbf{V_m}$ is the transmembrane potential at each node

$$\mathbf{V_m} = \left[\begin{array}{cccc|cc|cccc} V_m^{(1,1)} & V_m^{(1,2)} & \cdots & V_m^{(1,p)} & \cdots & \cdots & V_m^{(n,1)} & V_m^{(n,2)} & \cdots & V_m^{(n,p)} \end{array}\right]^{\mathsf{T}} \tag{47}$$

To consider additional myocytes coupled together at a single cleft, one can derive a slightly different form of the resistance matrix $\mathbf{R}$ and Laplacian matrix for computing the voltage vector $\mathbf{V}$. As an example, we provide the form of these matrices when two myocytes are coupled to a single myocyte at a common cleft.

$$\left[\begin{array}{cccccc|cccccc|cccccc}
R_5 & 0 & 0 & 0 & 0 & 0 & & & & & & & & & & & & \\
0 & R_0 & 0 & 0 & 0 & 0 & & & & & & & & & & & & \\
0 & 0 & R_0 & 0 & 0 & 0 & & & & & & & & & & & & \\
0 & 0 & 0 & R_0 & 0 & 0 & & & & & & & & & & & & \\
0 & 0 & 0 & 0 & R_0 & R_2 & R_4 & & & & & & R_4 & & & & & \\
0 & 0 & 0 & 0 & 0 & R_6 & R_3 & & & & & & R_3 & & & & & \\
\hline
 & & & & & R_3 & R_1 & 0 & 0 & 0 & 0 & 0 & & & & & & \\
 & & & & & R_4 & R_2 & R_0 & 0 & 0 & 0 & 0 & & & & & & \\
 & & & & & & 0 & 0 & R_0 & 0 & 0 & 0 & & & \mathbf{0} & & & \\
 & & & & & & 0 & 0 & 0 & R_0 & 0 & 0 & & & & & & \\
 & & & & & & 0 & 0 & 0 & 0 & R_0 & 0 & & & & & & \\
 & & & & & & 0 & 0 & 0 & 0 & 0 & R_5 & & & & & & \\
\hline
 & & & & & R_3 & & & & & & & R_1 & 0 & 0 & 0 & 0 & 0 \\
 & & & & & R_4 & & & & & & & R_2 & R_0 & 0 & 0 & 0 & 0 \\
 & & & & & & & & \mathbf{0} & & & & 0 & 0 & R_0 & 0 & 0 & 0 \\
 & & & & & & & & & & & & 0 & 0 & 0 & R_0 & 0 & 0 \\
 & & & & & & & & & & & & 0 & 0 & 0 & 0 & R_0 & 0 \\
 & & & & & & & & & & & & 0 & 0 & 0 & 0 & 0 & R_5
\end{array}\right] \tag{48}$$

where the variables R_0, R_1, R_2, R_3, R_4, and R_5 are as described by 39-44 while

$$R_6 = -\left(R_{radial} + \tfrac{1}{2}R_{cl} + \tfrac{1}{2}R_{myo} + \tfrac{R_{myo}R_{cl}}{2R_{gap}}\right) \tag{49}$$

and

$$\mathbf{V} = \left[\begin{array}{cccccc|cccccc|cccccc}
1 & -1 & 0 & 0 & 0 & 0 & & & & & & & & & & & & \\
-2 & 3 & -1 & 0 & 0 & 0 & & & & & & & & & & & & \\
0 & -1 & 2 & -1 & 0 & 0 & & & & & & & & & & & & \\
0 & 0 & -1 & 2 & -1 & 0 & & & & & & & & & & & & \\
0 & 0 & 0 & -2 & 3 & -1 & & & & & & & & & & & & \\
0 & 0 & 0 & 0 & -1 & \gamma & \beta & & & & & & \beta & & & & & \\
\hline
 & & & & & \beta & \alpha & -1 & 0 & 0 & 0 & 0 & & & & & & \\
 & & & & & & -2 & 3 & -1 & 0 & 0 & 0 & & & & & & \\
 & & & & & & 0 & -1 & 2 & -1 & 0 & 0 & & & \mathbf{0} & & & \\
 & & & & & & 0 & 0 & -1 & 2 & -1 & 0 & & & & & & \\
 & & & & & & 0 & 0 & 0 & -2 & 3 & -1 & & & & & & \\
 & & & & & & 0 & 0 & 0 & 0 & -1 & 1 & & & & & & \\
\hline
 & & & & & \beta & & & & & & & \alpha & -1 & 0 & 0 & 0 & 0 \\
 & & & & & & & & & & & & -2 & 3 & -1 & 0 & 0 & 0 \\
 & & & & & & & & \mathbf{0} & & & & 0 & -1 & 2 & -1 & 0 & 0 \\
 & & & & & & & & & & & & 0 & 0 & -1 & 2 & -1 & 0 \\
 & & & & & & & & & & & & 0 & 0 & 0 & -2 & 3 & -1 \\
 & & & & & & & & & & & & 0 & 0 & 0 & 0 & -1 & 1
\end{array}\right] \mathbf{V_m} \tag{50}$$

where $\alpha = 1 + \frac{R_{myo}}{2R_{gap}}$, $\beta = -\frac{R_{myo}}{2R_{gap}}$, and $\gamma = 1 + \frac{R_{myo}}{R_{gap}}$.

These simplified forms can be modified to incorporate additional biophysical detail and complexity. When considering heterogeneous GJ coupling and GJ gating for example, the term R_{gap} becomes $(R_{gap}^{i-1,i}/g^{i-1,i})$ where $R_{gap}^{i-1,i}$ is the resistance and $g^{i-1,i}$ is the gating variable for the GJ between myocytes $i-1$ and i. To consider heterogeneous myocyte dimensions, the term R_{myo} would need to be indexed appropriately for each myocyte $i \in \{1, \ldots, n\}$. Similarly, the terms R_{cl} and R_{radial} would need to be indexed appropriately when considering heterogeneous cleft dimensions.

Supplemental Figures

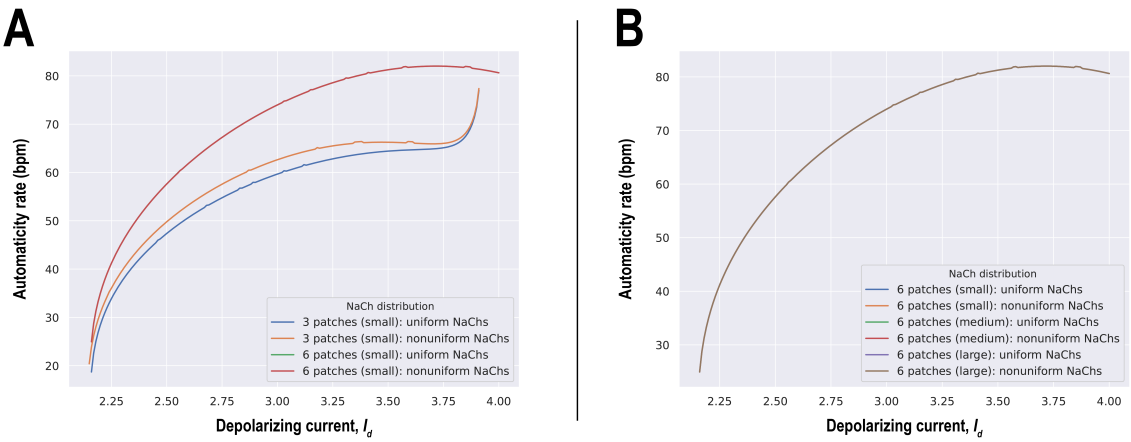

Figure S1: PSC-CM automaticity rate across different myocyte sizes and sodium channel (NaCh) distributions. **(A)** PSC-CM automaticity rate as a function of depolarizing current, I_d for when PSC-CMs were discretized into either 3 and 6 intracellular patches and NaChs were distributed uniformly or nonuniformly. Small PSC-CMs were cylindrical with radius = 6 µm and length = 18 µm **(B)** PSC-CM automaticity rate as a function of I_d across various sizes (small: radius = 6 µm, length = 18 µm); medium: radius = 8 µm, length = 40 µm); large: radius = 11 µm, length = 100 µm) and NaCh distributions.

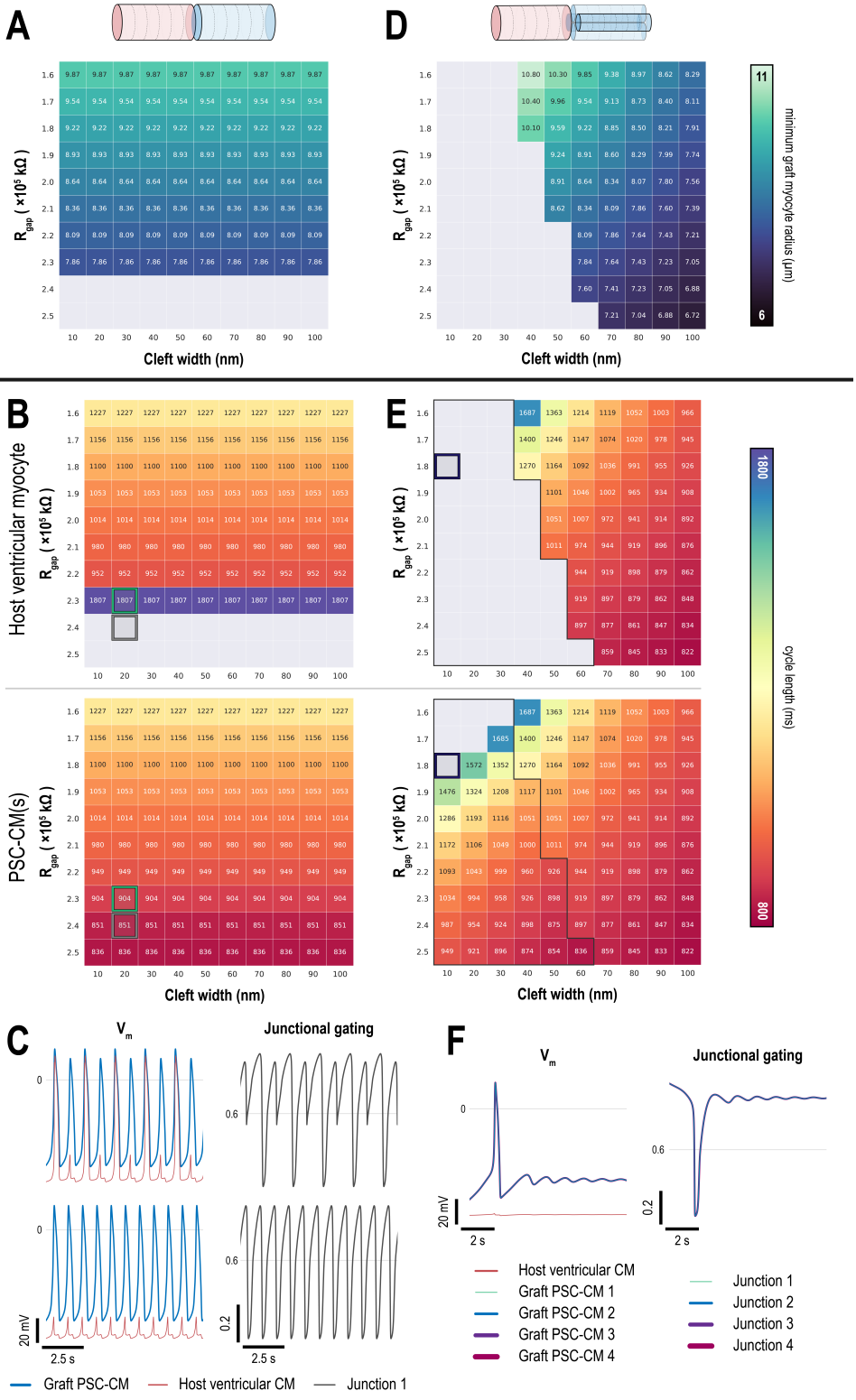
A
D
B
E
C
F
Host ventricular myocyte
PSC-CM(s)
R_{gap} (×10^5 kΩ)
Cleft width (nm)
minimum graft myocyte radius (μm)
cycle length (ms)
V_m
Junctional gating
20 mV
2.5 s
2 s
Graft PSC-CM
Host ventricular CM
Junction 1
Graft PSC-CM 1
Graft PSC-CM 2
Graft PSC-CM 3
Graft PSC-CM 4
Junction 2
Junction 3
Junction 4

Figure S2 *(previous page)*: The effect of electrotonic interactions between host and graft CMs on graft CM automaticity and the emergence and rate of graft-induced spontaneous ectopic beats in host CMs. **(A,D)** Minimum PSC-CM radius required to elicit a spontaneous ectopic beat in a host ventricular CM when coupled as either **(A)** 1:1 or **(D)** 1:4 host-graft tandems across combinations of gap junctional resistance (R_{gap}) and cleft width. In both cases, $I_d = 3.7$ μA/μF. In the 1:4 coupling configuration, initial states were synchronized across all PSC-CMs. **(B,E)** Heat maps show how the average cycle lengths of graft-induced ectopic beats in a host ventricular CM (top) and spontaneously beating graft PSC-CMs (bottom) change with R_{gap} and ID cleft width for **(B)** 1:1 and **(E)** 1:4 coupling configurations; graft PSC-CMs were the same size as the host CM. **(C,F)** Representative V_m traces of host and graft CMs (left) and junctional gating (right) for **(C)** 1:1 and **(F)** 1:4 coupling configurations; values of R_{gap} and cleft widths corresponding to traces are highlighted in panels **(B)** and **(E)**, respectively. In the 1:4 coupling configuration, the junction index corresponds to the corresponding graft PSC-CM index. **(C)** Instances of 2:1 capture were observed in the 1:1 coupling configuration (top), while **(F)** instances of complete suppression of PSC-CM automaticity were observed in the 1:4 coupling configuration.

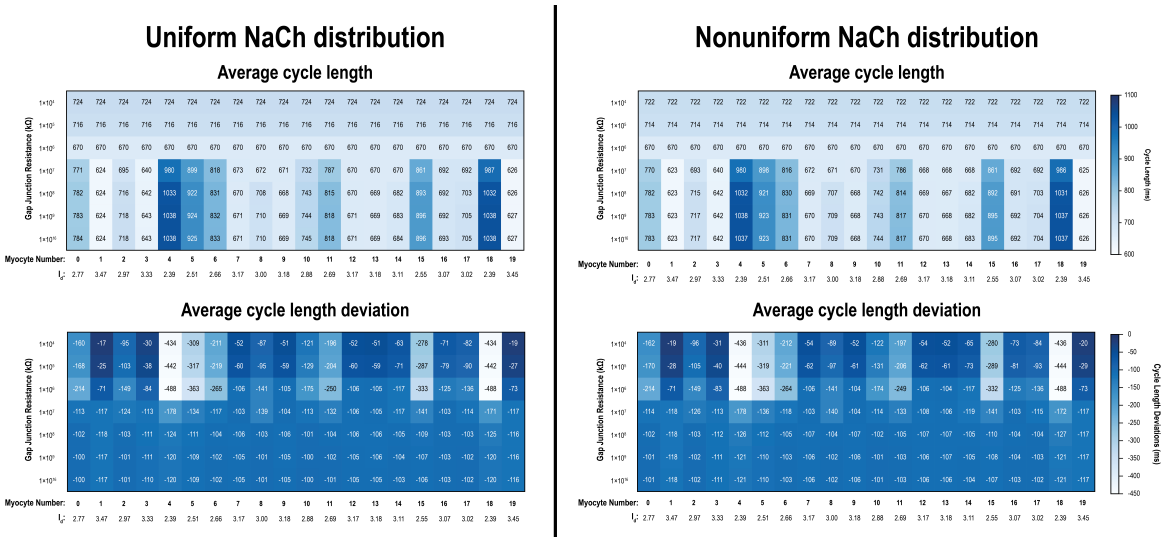

Figure S3: Additional PSC-CM cycle length results (cleft width = 10 nm). Average cycle lengths (top) and deviations (bottom) of 20 linearly coupled PSC-CMs (0-19) when NaChs were distributed either uniformly (left) or nonuniformly (right). Deviation in cycle length was computed relative to the cycle length of its corresponding isolated PSC-CM with the same I_d for each individual PSC-CM in the linear strand. Values of I_d are shown below each corresponding myocyte number.

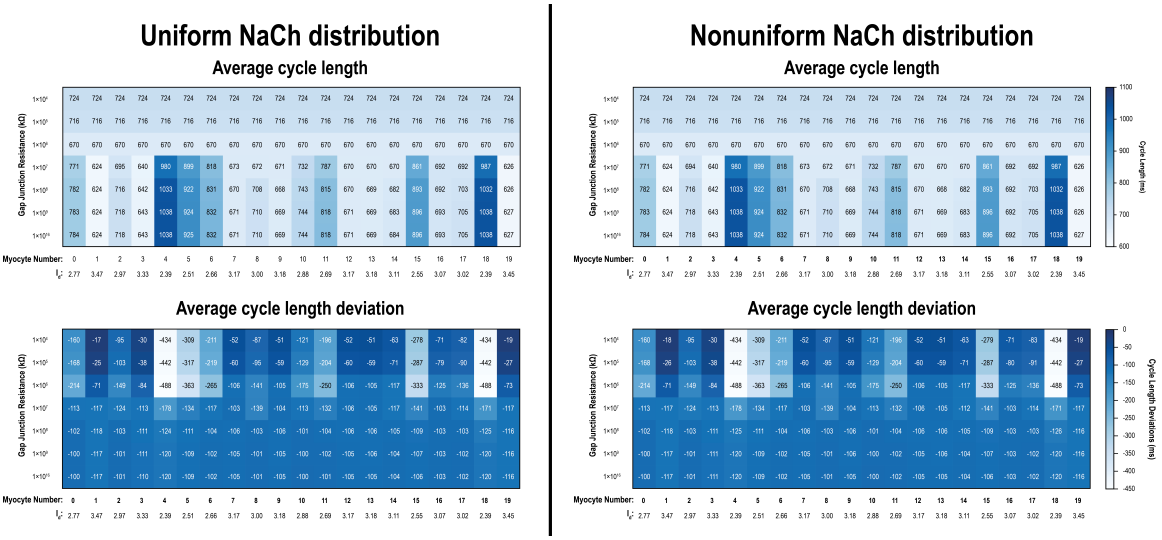

Figure S4: Additional PSC-CM cycle length results (cleft width = 100 nm). Average cycle lengths (top) and deviations (bottom) of 20 linearly coupled PSC-CMs (0-19) when NaChs were distributed either uniformly (left) or nonuniformly (right). Deviation in cycle length was computed relative to the cycle length of its corresponding isolated PSC-CM with the same I_d for each individual PSC-CM in the linear strand. Values of I_d are shown below each corresponding myocyte number.

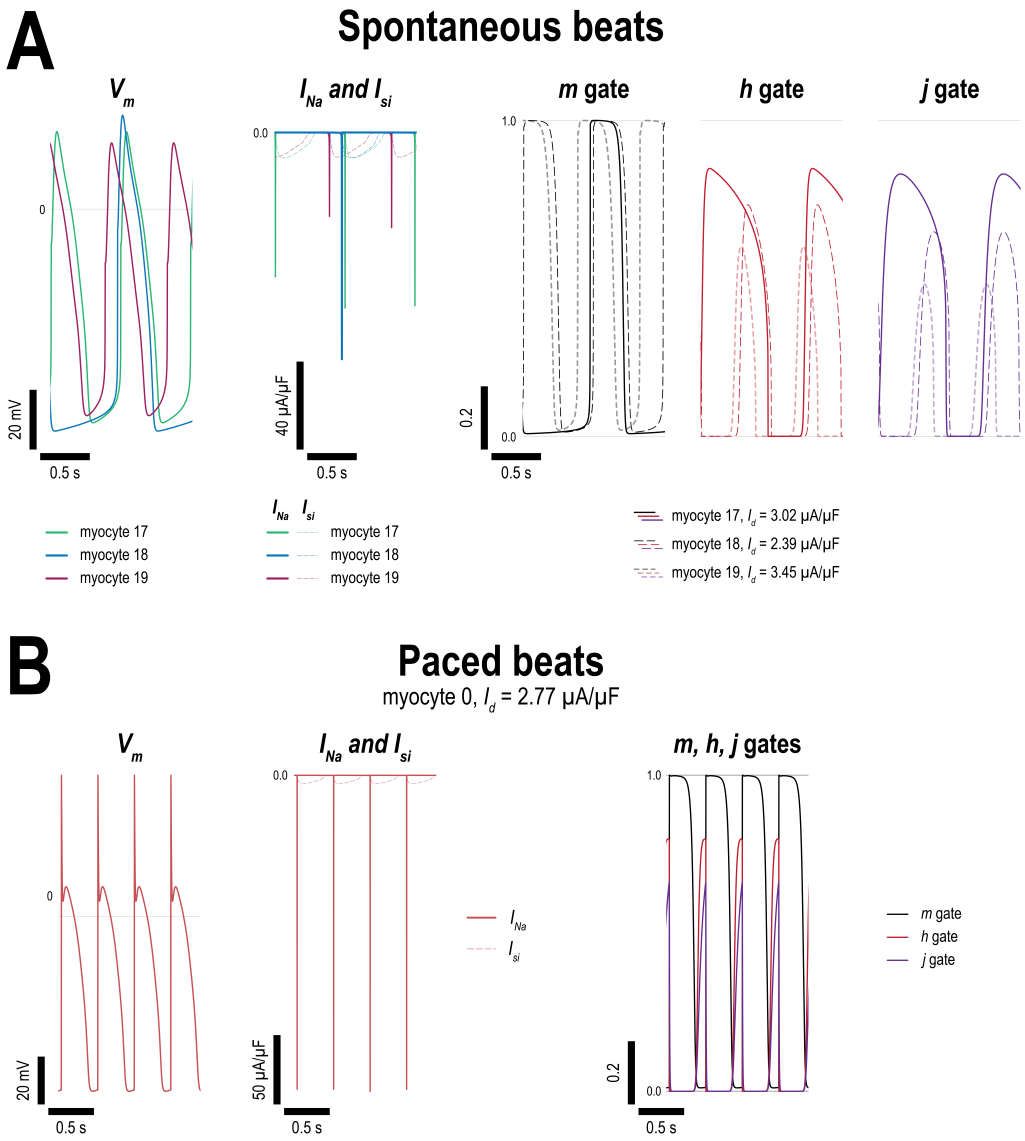

Figure S5: Depolarizing currents in spontaneous versus paced beats in PSC-CMs. Representative traces for V_m, depolarizing currents (I_{Na}, I_{si}), and I_{Na} gating variables (m, h, j) for **(A)** spontaneous and **(B)** paced beats (CL = 400 ms). Spontaneous beats are shown for myocytes 17, 18, 19 (I_d values of 3.02, 2.39, and 3.45 μA/μF, respectively); paced beats are of myocyte 0 ($_d$ = 2.77 μA/μF). Compared to paced beats, spontaneous beats exhibited reduced I_{Na} that depended on I_d. PSC-CMs with larger I_d had elevated maximum diastolic potentials that resulted in incomplete reactivation of I_{Na} inactivation gates (h, j).

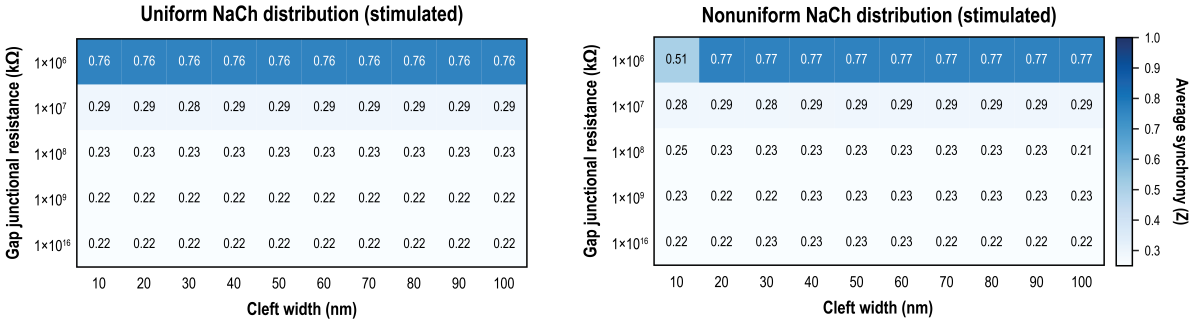

Figure S6: Average synchrony across linear strand of 20 PSC-CMs paced along one side. Heat maps of average synchrony across combinations of gap junctional resistances (R_{gap}) and cleft widths for 20 linearly coupled PSC-CMs with either uniform (left) and nonuniform (right) NaCh distributions. The myocardial strand was paced from myocyte 0 at a basic CL of 400 ms.

Computational model parameter values

Table 1: Parameter values for host and graft myocardium

Variable	**Name**	**Units**	**Value** Host myocardium	**Value** Graft myocardium
p	Number of patches	...	6	6
$L_p = L/(p-2)$	Axial patch length	μm	25	25
r	Myocyte radius	μm	11	$[6, 11]$
$C_{ax} = C_m(2\pi r L_p)$	Axial patch capacitance	μF	1.73×10^{-5}	$[9.42 \times 10^{-6}, 1.73 \times 10^{-5}]$
$C_{disc} = C_m(\pi r^2)$	Disc patch capacitance	μF	3.80×10^{-6}	$[1.13 \times 10^{-6}, 3.80 \times 10^{-6}]$
ρ_{myo}	Myoplastmic resistivity	Ω·cm	150	150
$R_{myo} = \rho_{myo} L_p/(\pi r^2)$	Myoplasmic resistance	kΩ	98.65	$[98.65, 331.57]$
ρ_{ext}	Extracellular resistivity	Ω·cm	150	150
w_c	Cleft width	nm	20	varied between $[10, 100]$
$R_{radial} = \rho_{ext}/(8\pi w_c)$	Radial cleft resistance	kΩ	2.98	varied between $[0.60, 2.98]$
$R_{cl} = \rho_{ext} w_c/(\pi r^2)$	Axial cleft resistance	Ω	78.91	varied based on w_c and r

Table 2: Parameter values for gap junctional gating model

Variable	**Description**	**Units**	**Value**
g_{min}	minimum value for g_∞	...	0.2
g_{max}	maximum value for g_∞	...	1.0
A_g	g_∞ parameter	mV^{-1}	0.09
V_g	g_∞ parameter	mV	50
σ_g	τ_g parameter	ms^{-1}	1.48×10^{-3}
k_g	τ_g parameter	mV^{-1}	0.0493

References

1. Kucera, J. P., Rohr, S. & Rudy, Y. Localization of sodium channels in intercalated disks modulates cardiac conduction. *Circ Res* **91,** 1176–82. ISSN: 1524-4571 (Electronic) 0009-7330 (Linking). https://www.ncbi.nlm.nih.gov/pubmed/12480819 (2002).
2. Greer-Short, A., George, S. A., Poelzing, S. & Weinberg, S. H. Revealing the Concealed Nature of Long-QT Type 3 Syndrome. *Circ Arrhythm Electrophysiol* **10,** e004400. ISSN: 1941-3084 (Electronic) 1941-3084 (Linking). https://www.ncbi.nlm.nih.gov/pubmed/28213505 (2017).
3. Tsumoto, K., Ashihara, T., Haraguchi, R., Nakazawa, K. & Kurachi, Y. Ischemia-related subcellular redistribution of sodium channels enhances the proarrhythmic effect of class I antiarrhythmic drugs: a simulation study. *PLoS One* **9,** e109271. ISSN: 1932-6203 (Electronic) 1932-6203 (Linking). https://www.ncbi.nlm.nih.gov/pubmed/25279776 (2014).
4. Luo, C. H. & Rudy, Y. A model of the ventricular cardiac action potential. Depolarization, repolarization, and their interaction. *Circ Res* **68,** 1501–26. ISSN: 0009-7330 (Print) 0009-7330 (Linking). https://www.ncbi.nlm.nih.gov/pubmed/1709839 (1991).
5. Kanakov, O. I., Osipov, G. V., Chan, C. K. & Kurths, J. Cluster synchronization and spatio-temporal dynamics in networks of oscillatory and excitable Luo-Rudy cells. *Chaos* **17,** 015111. ISSN: 1054-1500 (Print) 1054-1500 (Linking). https://www.ncbi.nlm.nih.gov/pubmed/17411268 (2007).
6. Stamp, A. T., Osipov, G. V. & Collins, J. J. Suppressing arrhythmias in cardiac models using overdrive pacing and calcium channel blockers. *Chaos* **12,** 931–940. ISSN: 1089-7682 (Electronic) 1054-1500 (Linking). https://www.ncbi.nlm.nih.gov/pubmed/12779617 (2002).
7. Tsumoto, K., Ashihara, T., Haraguchi, R., Nakazawa, K. & Kurachi, Y. Roles of subcellular Na+ channel distributions in the mechanism of cardiac conduction. *Biophys J* **100,** 554–563. ISSN: 1542-0086 (Electronic) 0006-3495 (Linking). https://www.ncbi.nlm.nih.gov/pubmed/21281569 (2011).
8. Weinberg, S. H. Ephaptic coupling rescues conduction failure in weakly coupled cardiac tissue with voltage-gated gap junctions. *Chaos* **27,** 093908. ISSN: 1089-7682 (Electronic) 1054-1500 (Linking). https://www.ncbi.nlm.nih.gov/pubmed/28964133 (2017).
9. Katz, B. *Nerve, muscle, and synapse* ix, 193 p. (McGraw-Hill, New York, 1966).
10. Stacey, R. G., Hilbert, L. & Quail, T. Computational study of synchrony in fields and microclusters of ephaptically coupled neurons. *J Neurophysiol* **113,** 3229–41. ISSN: 1522-1598 (Electronic) 0022-3077 (Linking). https://www.ncbi.nlm.nih.gov/pubmed/25673735 (2015).